Supplementary Information

Tunable bio-inspired hybrid hydrogels reprogram stem cell-derived extracellular vesicles for superior wound regeneration

Yen-Han Lai [1,2,3], Suhana[2,3,4], Su-Shin Lee[2,3,5], Ke-Hsun Yang[2,3,6], Yi-Chia Wu[2,3,5], Pavanchandh Atturu[2,3,4], Chung-Yuan Chan[4], Chih-Kuang Wang [1, 2,3,4,*]

[01] Graduate Institute of Medicine, College of Medicine, Kaohsiung Medical University, Kaohsiung, Taiwan

[02] Regenerative Medicine and Cell Therapy Research Center, Kaohsiung Medical University, Kaohsiung, Taiwan

[03] Orthopaedic Research Center, Kaohsiung Medical University, Kaohsiung, Taiwan

[04] Department of Medicinal and Applied Chemistry, College of Life Science, Kaohsiung Medical University, Kaohsiung, Taiwan

[05] Department of Surgery, College of Medicine, Kaohsiung Medical University, Kaohsiung, Taiwan

[06] Department of Biotechnology, College of Life Science, Kaohsiung Medical University, Kaohsiung, Taiwan

* Corresponding author: Chih-Kuang Wang
E-mail address: ckwang@kmu.edu.tw (C.K. Wang)
Tel.: 886-7-3121101 ext. 2677; Fax: 886-7-3125339

S1 ^{1}H NMR Analysis of Gelatin and Gelatin Methacryloyl (GelMA)

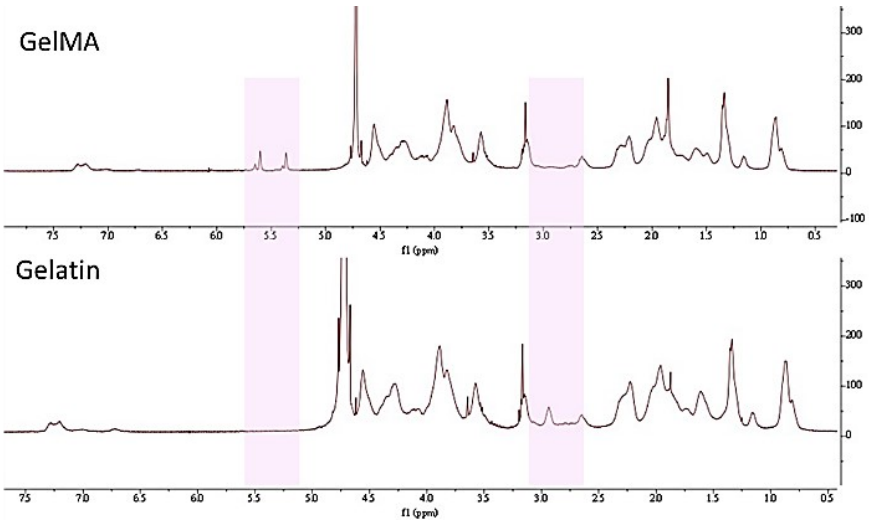

Fig. S1. ^{1}H NMR spectra of gelatin methacryloyl (GelMA).

Fig. S1 Comparing the ^{1}H NMR spectra of unmodified gelatin and methacrylated gelatin (GelMA). Native gelatin shows broad aliphatic proton signals between 0.8-4.5 ppm and characteristic aromatic protons of phenylalanine (Phe) at 7.1-7.4 ppm. After methacrylation, the GelMA spectrum exhibits two new sets of peaks that are absent in gelatin: vinyl protons of the methacryloyl group at 5.4-6.0 ppm (CH_2=CH–), and methyl protons of the methacryloyl group at 1.8-2.0 ppm (–C(CH_3)=CH_2). The appearance of these peaks confirms successful grafting of methacryloyl groups onto gelatin lysine residues, consistent with earlier reports on GelMA synthesis. Moreover, the lysine ε–CH_2 proton region (≈3.0-3.2 ppm) decreases relative to the Phe aromatic signal, indicating consumption of primary amines, which is the main reaction site during GelMA formation.

The degree of methacrylation (DoM) was quantified by comparing the decrease of the lysine ε–CH_2 resonance (3.0-3.2 ppm), normalized to the phenylalanine (Phe) aromatic protons (7.1-7.4 ppm), following the methods reported by Van Den Bulcke et al [s1] and Sreekumaran et al [s2]. The normalized lysine-to-Phe ratios were 0.352 for native gelatin and 0.0235 for GelMA. Applying Eq. (S1), the resulting DoM was calculated as:

$$R_{\mathrm{Gelatin}} = \frac{I_{\mathrm{Lys}}^{\mathrm{Gelatin}}}{I_{\mathrm{Phe}}^{\mathrm{Gelatin}}} = \frac{1.84}{5.23} = 0.352 \quad ; \quad R_{\mathrm{GelMA}} = \frac{I_{\mathrm{Lys}}^{\mathrm{GelMA}}}{I_{\mathrm{Phe}}^{\mathrm{GelMA}}} = \frac{0.12}{5.10} = 0.0235$$

$$DoM = \left[1 - \frac{0.0235}{0.352}\right] \times 100 = 93.3\% \qquad \text{(S1-1)}$$

This indicates that over **93%** of the primary amines on gelatin were substituted by methacrylamide groups, consistent with a highly methacrylated GelMA. Such a high DoM is expected to yield a densely photo-crosslinked network with increased stiffness, reduced swelling, and enhanced structural integrity.

S2 ^{1}H NMR Analysis of Hyaluronic Acid and Hyaluronic Acid Methacryloyl (HAMA)

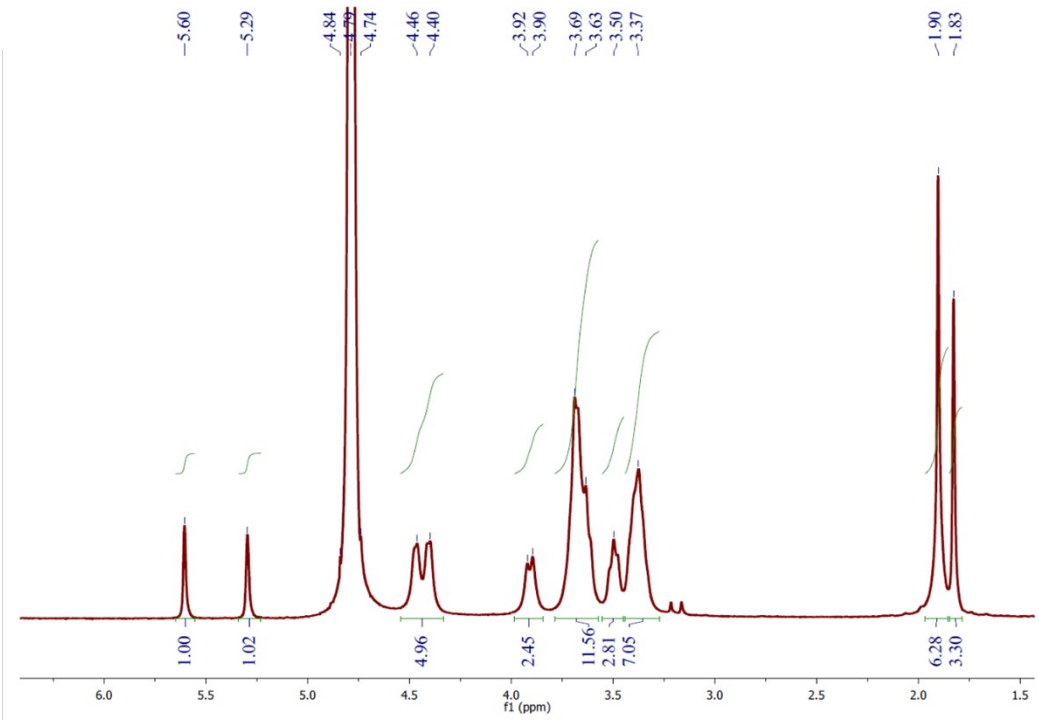

Fig. S2. H NMR spectra of hyaluronic acid methacryloyl (HAMA).

Fig. S2 shows the ^{1}H NMR spectra of native HA and HAMA. Native HA displays ring protons at 3.0-4.0 ppm, and N-acetyl methyl protons at 1.9 ppm. After methacrylation, HAMA shows new characteristic signals: vinyl protons at 5.6-6.3 ppm and methacrylate methyl protons at 1.8-2.0 ppm. The degree of substitution (DoS) of HAMA was determined from the ^{1}H NMR spectrum by integrating the methacrylate vinyl protons (δ ≈ 5.5-5.2 ppm) and the N-acetyl methyl protons of HA (δ ≈ 1.9 ppm), following previously reported methods for methacrylated hyaluronic acid [s3,s4]. The CH_2 (δ ≈ 5.6 ppm, 2H) and CH (δ ≈ 5.2 ppm, 1H) resonances of the methacrylate group showed integrals of 1.00 and 1.02, respectively, while the N-acetyl methyl signal integrated to (6.28). The degree of substitution (DoS) of methacrylated hyaluronic acid (HAMA) was quantified by entire-vinyl method:

$$DoS = \frac{I_{vinyl}/2}{I_{NAc}/3} \times 100\%$$

This method is widely adopted in the literature because the methacrylate vinyl moiety contains two protons and the N-acetyl methyl group provides an internal standard of three protons per disaccharide unit. The DoS was then obtained from

$$DoS(\%) = \frac{(2.02)/2}{(6.28)/3} \times 100,$$

giving a degree of methacrylation of approximately **47.8%** for HAMA.

However, the degree of substitution of HAMA was also additionally quantified by comparing the methacrylate methyl resonance (δ ≈ 1.80 ppm, 3H) with the intrinsic N-acetyl methyl resonance of HA (δ ≈ 1.90 ppm, 3H) [s5]. From the measured integrals ($I_{MA\text{-}CH_3}$) = 3.30 and I_{NAc} = 6.28, the DoS was calculated as

$$DoS = (\frac{I_{MA-CH_3}}{I_{NAc}}) \times 100,$$

yielding a methacrylation degree of **≈52.5%**. This result is consistent with the high level of functionalization observed from the vinyl-region analysis and confirms that the synthesized HAMA possessed a high density of photo-crosslinkable methacrylate groups.

The above analysis of the structure and modification rate of HAMA shows that the modification rate should be between 47.8% and 52.5%, which is a moderate-to-high modification rate. This confirms that the synthesized HAMA possesses a moderate-to-high density of photo-crosslinkable methacrylate groups.

S3 ^{1}H NMR Analysis of Polyethylene glycol diacrylate (PEGDA-8000 Da)

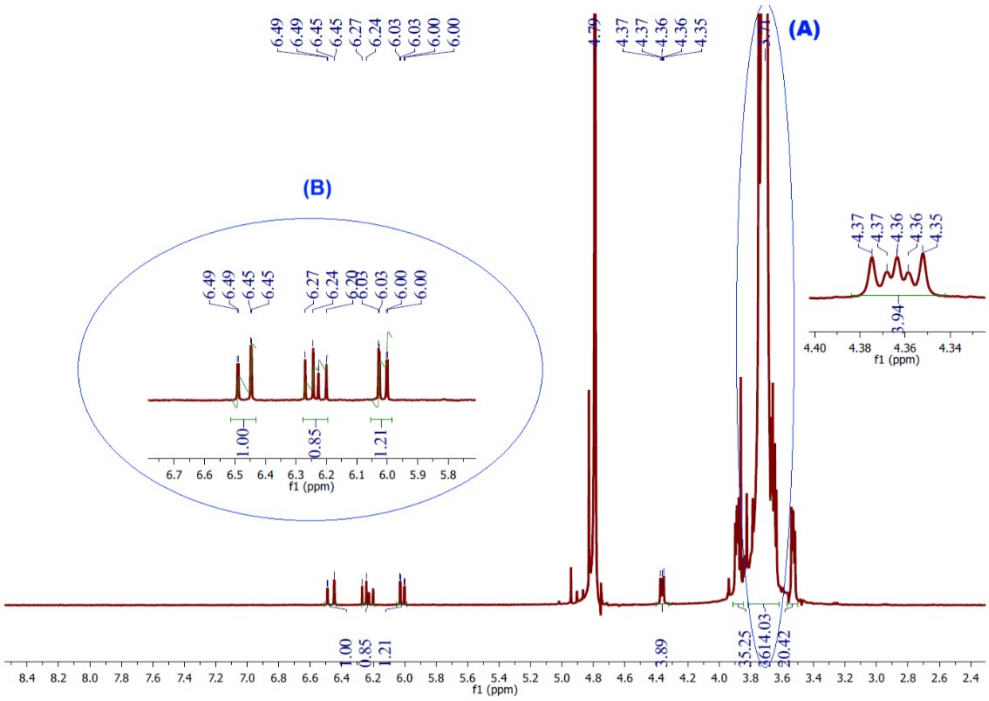

Fig. S3. H NMR spectra of polyethylene glycol diacrylate (PEGDA).

Polyethylene glycol diacrylate (PEGDA) was synthesized by reacting hydroxyl-terminated PEG (Mn≈ 8000 Da) with acryloyl chloride under anhydrous conditions to introduce acrylate ester groups at both polymer chain ends. Fig. S3 shows the 1H NMR spectrum of the resulting PEGDA-8000. Successful acrylation is confirmed by the appearance of the characteristic vinyl proton signals of the acrylate group at δ 6.49, 6.21, and 6.00 ppm, corresponding respectively to the trans-, cis-, and geminal protons of the –CH_2=CH–COO– moiety. These three peaks appear in the expected 1:1:1 ratio, consistent with terminal acrylate functionality. The PEG backbone resonance at δ 3.60-3.75 ppm remains unchanged, whereas the ester-adjacent methylene protons at δ 4.25-4.35 ppm emerge following acrylation, further confirming successful end-group esterification.

To quantify the degree of acrylation (DoA), the integrals of the acrylate vinyl protons (B) were compared to the integrals of the PEG backbone methylene protons (A), following established approaches in PEGDA [s6-8]. For PEG, each oxyethylene unit (–O–CH_2–CH_2–) contains four methylene protons, while each acrylate group contributes three vinyl protons, giving six total vinyl protons for di-acrylated PEGDA. The theoretical proton ratio under complete acrylation is therefore:

$$\left(\frac{B}{A}\right)_{\text{theoretical}} = \frac{6}{4n}$$

where $n = M_{\text{PEG}}/44$ is the number of PEG repeating units. For PEG-8000, $n = 8000/44 \approx 182$, yielding:

$$\left(\frac{B}{A}\right)_{\text{theoretical}} = \frac{6}{728} = 0.00824.$$

From the NMR spectrum (Fig. S3), the vinyl proton integrals were 0.33, 0.24, and 0.34, giving $B = 3.06$. The PEG backbone region was integrated as $A = 614.03$, which corresponds to the integrals of the PEG backbone methylene protons. The experimental ratio is therefore:

$$\left(\frac{B}{A}\right)_{\text{exp}} = \frac{3.06}{614.03} = 0.00498$$

$$\text{DoA}(\%) = \frac{(B/A)_{\text{exp}}}{(B/A)_{\text{theoretical}}} \times 100 = \frac{0.00498}{0.00824} \times 100 \approx 60.5\%$$

The resulting DoA of approximately **60.5%** indicates that most of the PEG chain termini were successfully acrylated. This finding is consistent with previously reported observations that PEG macromers with high molecular weight (≥6000 Da) exhibit substantially reduced acrylation efficiency compared to low-molecular-weight PEG. Sawhney et al. reported that PEGDA-6000 typically achieves 70-80% acrylation, whereas PEGDA-10000 often falls to 30-60% [s6]. Peter et al. likewise demonstrated a sharp decrease in conversion for PEGDA-8000 relative to PEGDA-3400, despite identical reaction conditions [s7]. This reduced reactivity is attributed to the very low end-group concentration in high-molecular-weight PEG, the hydration shell and dynamic coil structure of long PEG chains that sterically shield hydroxyl end-groups, and the competing formation of mono-acrylated PEG rather than di-functional PEGDA [s8]. Commercial suppliers similarly report that PEGDA-700 and PEGDA-3400 are typically >90% acrylated, whereas PEGDA-8000 and higher are often only partially acrylated (60-80%) even under optimized synthesis conditions. In summary, this study achieved a PEGDA modification rate of 60.5%, enabling crosslinking of double bonds through PEG-terminated acrylate groups.

(a)

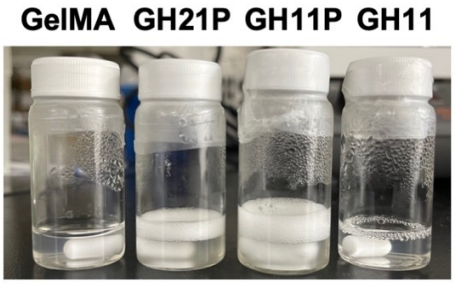

(b)

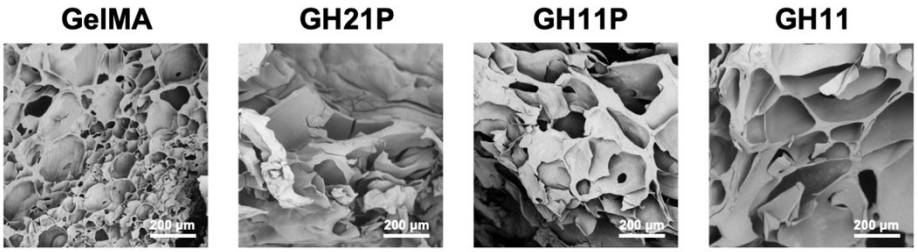

Fig. S4. Macroscopic appearance and microstructure of hydrogel formulations. (a) Macroscopic images of four hydrogel solutions at 15% (w/v): GelMA, GH21P, GH11P, and GH11 formulations before and after photo-crosslinking. (b) Cross-sectional SEM images of freeze-dried hydrogels revealing internal porous microstructure. Scale bars: 100 µm.

(a) Representative scatter plots

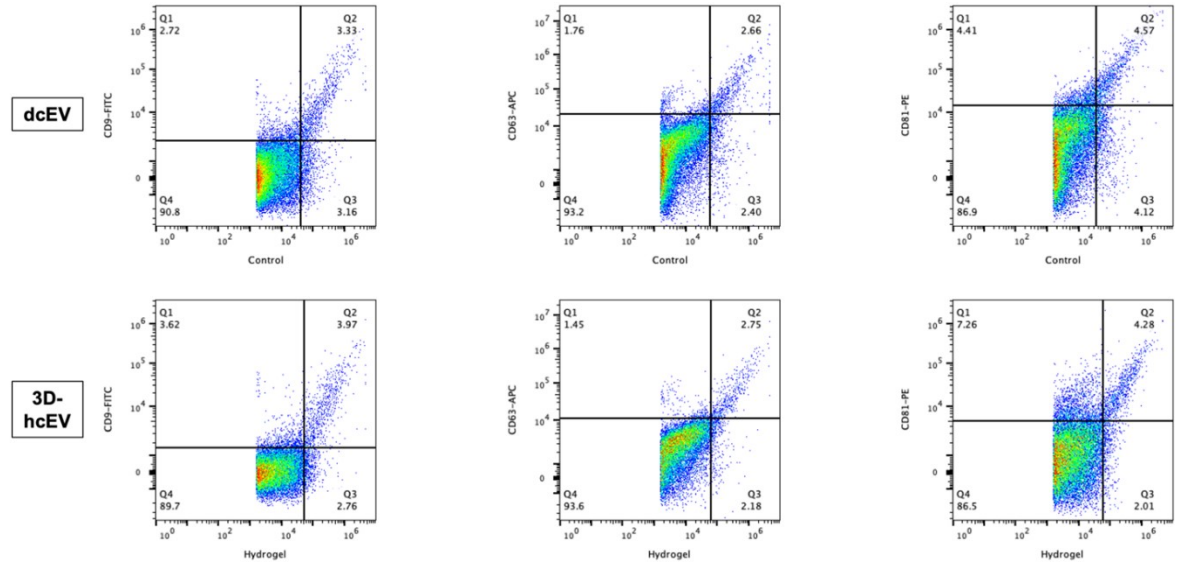

(b) Control validation

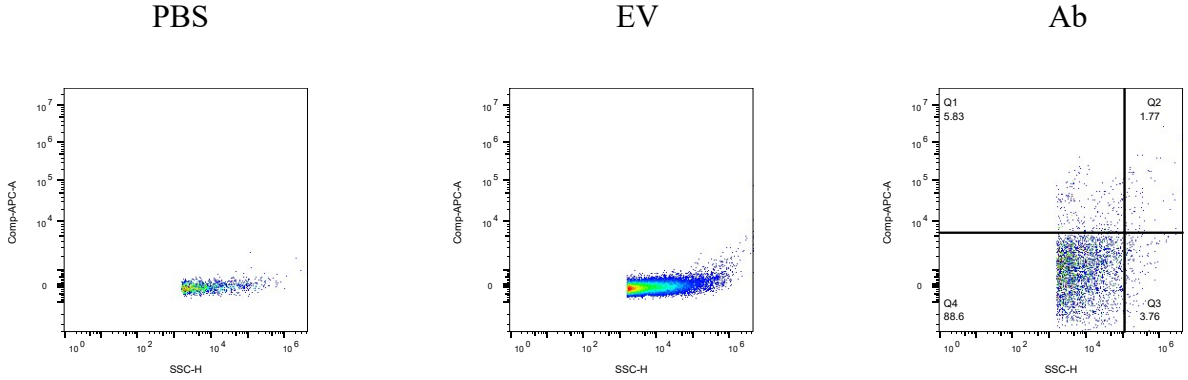

Fig. S5. Single-particle flow cytometric analysis of tetraspanin expression in 2D dish cultured EV (dcEV) and 3D hydrogel (GH11P) cultured EV (3D-hcEV). (a) Representative scatter plots from single-particle flow cytometry showing SSC-A (side scatter area) versus fluorescence intensity for CD9-FITC, CD63-APC, and CD81-PE. Gating was performed to include particles ≥100 nm based on SSC-A threshold while excluding background noise, doublets, and aggregates. All axes are displayed on a logarithmic scale. (b) Control validation plots used to establish compensation and gating thresholds. From left to right: PBS buffer only (PBS control), unstained EVs (EV control), and single-antibody control (EV + antibody only). These controls define baseline fluorescence and confirm that the main tetraspanin-positive populations observed in panel (a) arise from specifically labeled EVs rather than background or nonspecific antibody binding.

Single-particle analysis was performed on a Cytek Aurora spectral flow cytometer (Cytek Biosciences, Fremont, CA). Spectral unmixing and compensation were applied in FlowJo (Becton Dickinson). Tetraspanin-positive EVs were defined as SSC-A^{+} events within the EV gate exceeding fluorescence thresholds established by negative controls. All samples were analyzed in triplicate.

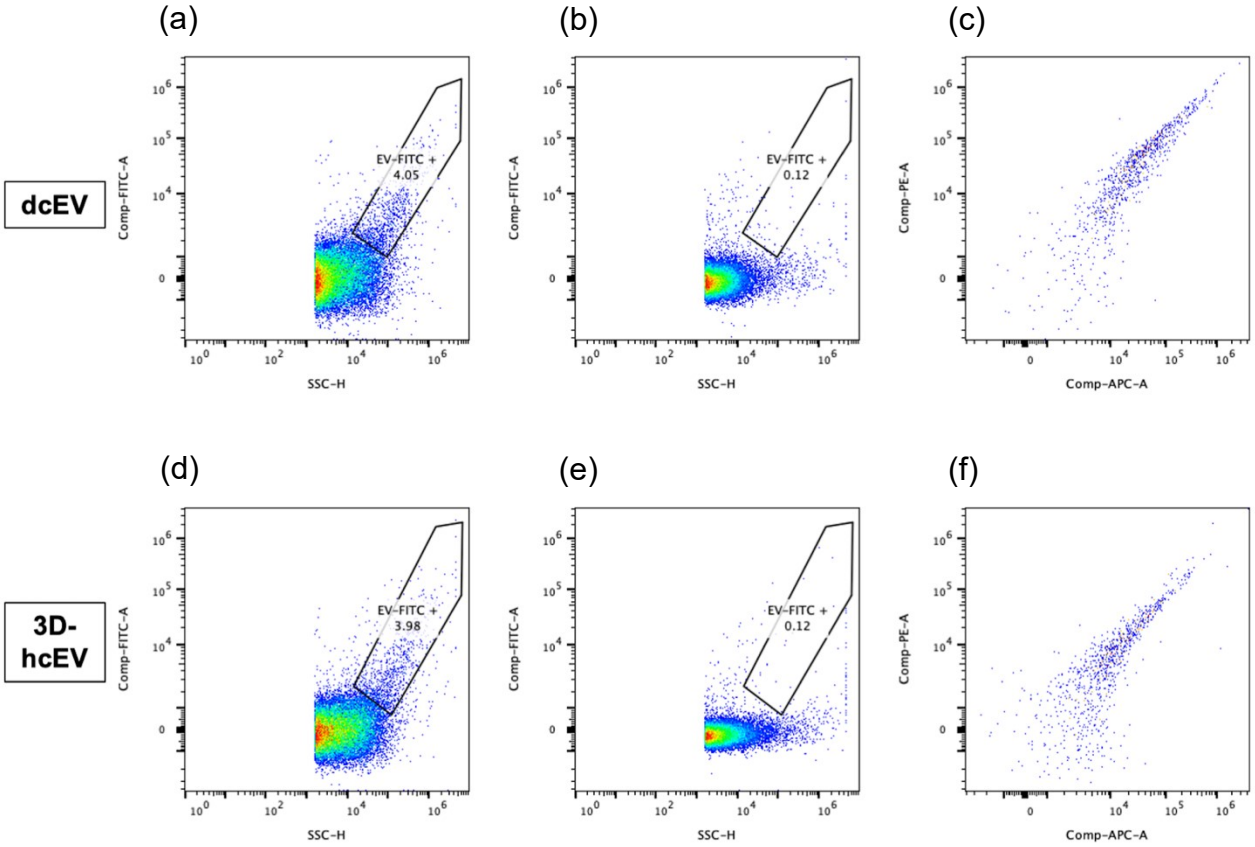

Fig. S6. Detergent-lysis control to support membrane-enclosed EV events in single-particle flow cytometry.

The dcEV and 3D-hcEV samples were labeled with anti-CD9-FITC and analyzed by spectral flow cytometry using the same acquisition and gating strategy. In untreated samples (Fig. S6a,d), a CD9-positive event population was detected within the predefined EV gate (approximately 4.05% for dcEV and 3.98% for 3D-hcEV). Following detergent treatment (Triton X-100, 1%, 30 min, 4 °C), the gated CD9-positive events were markedly reduced to ~0.12% in both groups (Fig. S6b,e), supporting that the detected CD9-associated signals largely originated from detergent-sensitive, membrane-enclosed particles rather than detergent-resistant non-vesicular artifacts. Panels (Fig. S6c,f) show the corresponding signal distribution in additional fluorescence channels (PE and APC) under the same acquisition settings. This lysis assay is consistent with MISEV2023 recommendations for EV characterization and appropriate controls [s9].

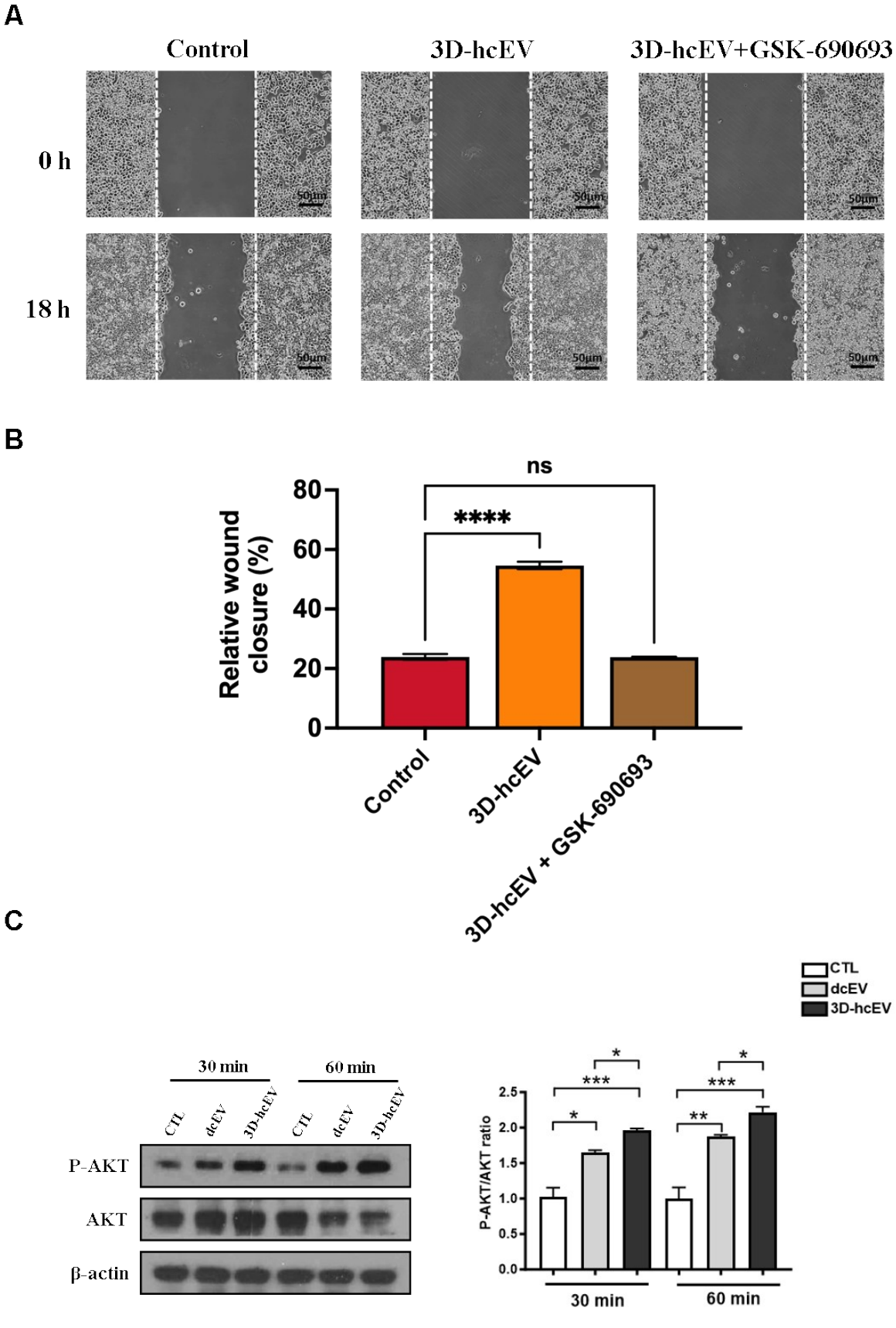

Figure S7. 3D-hcEVs promote HaCaT keratinocyte migration via AKT signaling. (A)

Representative images of the wound-healing assay in HaCaT keratinocytes treated with control (CTL), 3D-hcEVs, or 3D-hcEVs plus AKT inhibitor for 18 h. Scale bar = 50 μm. **(B)** Quantitative analysis of wound closure rate (%). Data are presented as mean ± SD (n = 3 independent experiments). **(C)** Western blot analysis of phosphorylated AKT (p-AKT) and total AKT levels in HaCaT cells after treatment with dcEVs or 3D-hcEVs for 30 or 60 min. β-actin served as the loading control. The right panels show the quantified p-AKT/AKT ratio. Statistical analysis: one-way ANOVA with Tukey's post hoc test. *$p < 0.05$, **$p < 0.01$, ***$p < 0.001$ versus CTL; #$p < 0.05$ between dcEV and 3D-hcEV groups.

Supplementary Tables

Table S1. Absence of intracellular organelle markers in 3D-hcEVs.

Marker category	Protein name	Gene symbol	Detection status in 3D-hcEVs
Endoplasmic Reticulum	Calnexin	CANX	Not Detected
	GRP94 (Endoplasmin)	HSP90B1	Not Detected
Golgi Apparatus	GM130	GOLGA2	Not Detected
Mitochondria	Cytochrome C	CYCS	Not Detected
Nucleus	Histones (H1/H2/H3)	HIST1H	Not Detected

Note: "Not Detected" indicates that protein levels were below the detection limit of the mass spectrometry analysis, confirming the high purity of the isolated extracellular vesicles.

To evaluate the purity of extracellular vesicles isolated from the hybrid hydrogel system, unbiased proteomic profiling was performed on 3D-hcEV lysates. This table summarizes the detection status of canonical markers for major intracellular organelles, including the endoplasmic reticulum (ER), Golgi apparatus, mitochondria, and nucleus. As indicated, these non-vesicular contaminants were consistently below the detection limit, supporting the exclusion of cellular debris in accordance with MISEV2023 guidelines.

References for Supplementary Material

[s1] Van Den Bulcke, A. I.; Bogdanov, B.; De Rooze, N.; Schacht, E. H.; Cornelissen, M.; Van Den Bulcke, A. I.; Bogdanov, B.; De Rooze, N.; Schacht, E. H.; Cornelissen, M.; Berghmans, H., Structural and Rheological Properties of Methacrylamide Modified Gelatin Hydrogels. Biomacromolecules 2000, 1 (1), 31–38.

[s2] Sreekumaran, S. S.; Radhakrishnan, A.; Rauf, A. A.; Kurup, G. M., Nanohydroxyapatite Incorporated Photocrosslinked Gelatin Methacryloyl/Poly(ethylene Glycol) Diacrylate Hydrogel for Bone Tissue Engineering. Prog. Biomater. 2021, 10, 43–51.

[s3] Patterson, J.; Siew, R.; Herring, S. W.; Lin, A. S.; Guldberg, R.; Stayton, P. S., Hyaluronic Acid Hydrogels with Controlled Degradation Properties for Oriented Bone Regeneration., Biomaterials 2010, 31 (26), 6772–6781.

[s4] Nedunchezian, S.; Wu, C.-W.; Wu, S.-C.; Chen, C.-H.; Chang, J.-K.; Wang, C.-K., Characteristic and Chondrogenic Differentiation Analysis of Hybrid Hydrogels Comprised of Hyaluronic Acid Methacryloyl (HAMA), Gelatin Methacryloyl (GelMA), and the Acrylate-Functionalized Nano-Silica Crosslinker. Polymers 2022, 14 (10), 2003.

[s5] Tavsanli, B.; Can, V.; Okay, O., Mechanically Strong Triple Network Hydrogels Based on Hyaluronan and Poly(N,N-dimethylacrylamide)., Soft Matter 2015, 11 (43), 8517–8524.

[s6] Sawhney, A. S.; Pathak, C. P.; Hubbell, J. A., Bioerodible Hydrogels Based on Photopolymerized Poly(ethylene glycol)-Co-Poly(α-Hydroxy Acid) Diacrylate Macromers., Macromolecules 1993, 26 (4), 581–587.

[s7] Peter, M.; Tayalia, P., An Alternative Technique for Patterning Cells on Poly(ethylene glycol) Diacrylate Hydrogels., RSC Adv. 2016, 6 (47), 40878–40885.

[s8] Zhao, X.; Lang, Q.; Yildirimer, L.; et al., Photocrosslinkable Gelatin for Epidermal Tissue Engineering., Adv Healthc Mater. 2016, 5(1), 108–18.

[s9] Welsh JA, Goberdhan DCI, O'Driscoll L, Buzas EI, Blenkiron C, Bussolati B, et al. Minimal information for studies of extracellular vesicles (MISEV2023): From basic to advanced approaches. J Extracell Vesicles. 2024;13(2):e12404.